Near-infrared light photocatalysis with metallic/semiconducting H_xWO_3/WO_3 nanoheterostructure in situ formed in mesoporous template

CrossMark

Ling Zhang, Wenzhong Wang[*], Songmei Sun, Dong Jiang

State Key Laboratory of High Performance Ceramics and Superfine Microstructures, Shanghai Institute of Ceramics, Chinese Academy of Sciences, 1295 Dingxi Road, Shanghai 200050, PR China

A B S T R A C T

In recent years, finding novel photocatalysts that can operate at a broad range of wavelengths is interesting in photocatalytic research filed. Here, a metallic/semiconducting H_xWO_3/WO_3 nanoheterostructure is prepared with ability to degrade organic dyes and to produce photocurrent under visible and near-infrared (NIR) irradiation. The metallic H_xWO_3 is helpful for electrons transfer then to enhance photocatalytic activity. The H_xWO_3/WO_3 nanoheterostructure exhibits excellent photoelectric conversion characteristics in infrared wavelength range. Strong interfacial contact between two components is advantaged for fabrication of photovoltaic device, indicating its potential application as an infrared photovoltaic cell.

© 2014 Elsevier B.V. All rights reserved.

1. Introduction

In view of solar energy utilization, searching a semiconductor that can harvest wide spectrum of solar light, from ultraviolet (UV) to near-infrared (NIR) wavelength, undoubtedly remains an urgent challenge for achieving efficient solar energy conversion. In addition, separation and transfer of photogenerated electrons (e^-) and holes (h^+) play key roles in determining the solar energy conversion efficiency of semiconductor-based photocatalyst [1]. Energy band modification by introducing dopant atoms into the photocatalysts has shown great potential to increase visible-light absorption. However, most doped systems suffered from serious recombination of photoexcited charge carriers [2,3]. It is still a challenge to increase photocatalytic activity for the broad spectrum responsive photocatalysts.

Recently, nanosized tungsten bronzes (M_xWO_3, M=H, Li, Na, K) have been identified as materials of high interest for commercial applications involving absorption of near-infrared (NIR) radiation (800–2500 nm) [4–6], especially in comparison to current benchmark materials including lanthanum hexaboride, indium doped tin oxide, and antimony doped tin oxide. Among the tungsten bronzes, hydrogen tungsten bronze (H_xWO_3, x in the range from 0.1 to 0.6) is known due to highly conductivity and a broad optical absorption band in the visible to near-infrared region arising from "chemichromic" effect [7]. More important, these materials also show very interesting electronic properties due to its metallic conductivity produced by electron mobility [8,9]. The metallic property means that carriers will be efficiently transferred to surface to involve in redox reaction.

Inspired from this metallic conductivity, we apply an approach to in situ synthesize H_xWO_3/WO_3 nanoheterostructure in mesoporous SiO_2 matrix template. As a Co-catalyst, H_xWO_3 might play a dual role in improving photocatalytic activity by not only promoting the separation and transfer of photoexcited charge carriers, but also increasing NIR light absorption. Furthermore, structures of tungsten oxide and tungsten bronze are quite similar [6], strong interfacial contact between the two materials will inevitably exert an obvious influence on the electronic structure of the photocatalyst, which has been considered as a efficient way to promote the separation of electrons and holes.

2. Experimental

2.1. Preparation of H_xWO_3/WO_3 nanoheterostructure

In a typical synthesis of mesocellular foam (MCF) template [10], 0.26 g of Pluronic F127 and 0.65 g of FC-4 ($C_3F_7O(CFCF_3CF_2O)_2CFCF_3CONH(CH_2)_3N^+(C_2H_5)_2CH_3I^-$) were dissolved in 30 ml of HCl solution (0.02 M), followed by the introduction of 0.30 g of 1,3,5-trimethylbenzene (TMB). After being

---

* Corresponding author. Tel.: +86 21 5241 5295; fax: +86 21 5241 3122.
   E-mail address: wzwang@mail.sic.ac.cn (W. Wang).

stirred for 2 h, 1.5 g of tetraethyl orthosilicate (TEOS) were added. Then the solution was stirred at 30 °C for 24 h, transferred to an autoclave, and kept at 100 °C for 24 h. The as-synthesized material was collected by centrifuge, dried in air, and heat treated at 550 °C for 5 h for surfactant removal before used as the template.

Hybrid H_xWO_3/WO_3 was prepared by a hard template replicating method. Typically, 0.27 g of 12-phosphotungstic acid (AR, Sinopharm) was dissolved in 10 ml of ethanol. Then 0.2 g of the as-prepared MCF template was added into the above solution under stirring at room temperature. After the solvent was evaporated gradually, white pulpy powder was obtained. The powder was calcined at 550 °C for 5 h to give a decomposed product of tungsten oxide inside the silica template. The silica template was removed by 2 M NaOH solution under stirring. After washing with enough de-ionized water and drying at room temperature in air, the H_xWO_3/WO_3 nanoheterostructure sample was obtained.

For comparison, monoclinic WO_3 was prepared by traditional hydrothermal synthesis [11]. The precursor was prepared by dissolving 2.0 g sodium tungstate dihydrate ($Na_2WO_4 \cdot 2H_2O$) as tungsten source in 50 ml of 6 M HCl solution under 30 min stirring to form H_2WO_4 solution. Then 30 ml of 1.50 g ammonium nitrate (NH_4NO_3) solution for controlling monoclinic structure was mixed in the solution for the synthesis of WO_3 nanoplates. The precursor solution was transferred into 100 ml teflon-lined stainless steel autoclave, which was processed at 200 °C for 24 h in an electric oven. At the completion of the process, the resulting precipitate of light-yellow (nanoplates) was separated by filtering, washed with distilled water to remove the remaining ions and ethanol to facilitate the evaporation of water, and finally dried at 100 °C in air for 12 h.

2.2. Characterizations

The crystal structures were recorded using a Rigaku D/max-2500 X-ray diffractometer (XRD) equipped with a Cu Kα irradiation source. A PerkinElmer Lambda 900 UV/vis/NIR double-beam spectrophotometer with an integrating sphere was used for diffuse reflectance measurements. The photoluminescence (PL) spectra were measured with a Hitachi F4600 fluorescence spectrophotometer at room temperature (excitation wavelength = 340 nm). The morphologies and microstructures of the as-prepared samples were investigated by transmission electron microscopy (TEM, JEOL JEM-2100F). Fourier transform infrared (FTIR) spectra were recorded on a Nicolet 8700 FTIR spectrometer (Thermo Scientific) with a spectral resolution of $2 \, cm^{-1}$. For in situ Raman measurements, the as-prepared samples powder were hand pressed on a glass substrate by a flat spoon. Thermo Scientific DXR Raman Analyzer was used in a backscattering-collection configuration at room temperature in air under the irradiation of the 535 nm diode laser.

2.3. Photocatalytic reactions and photocurrent measurements

The photocatalytic activity of the H_xWO_3/WO_3 nanoheterostructure was investigated by the photodegradation of methyl orange (MO, 10 mg/L). In a typical measurement, 50 ml of an aqueous suspension of MO and 50 mg of the heterostructure powders were placed in a 100 ml beaker. Prior to photoirradiation, the suspensions were magnetically stirred in the dark for 1 h to establish adsorptiondesorption equilibrium between the dye and the surface of the catalysts under ambient conditions. A 500 W Xe arc lamp as the light source and the appropriate light were obtained by filtering out IR or visible components with the filters ($\lambda < 760$ nm) or ($\lambda < 760$ nm). A 630 nm LED (3 W), 808 nm laser were used as the single light source. At varied irradiation time intervals, an aliquot of the mixed solution was collected and centrifuged, and the residual MO concentration in the supernatant

was analyzed by UV–vis spectroscopic measurements (Hitachi UV-3100).

Electrochemical measurements were performed on a CHI 660D electrochemical workstation (Shanghai Chenhua, China) using a standard three-electrode cell with a working electrode, a platinum wire as counter electrode, and a standard saturated calomel electrode (SCE) in saturated KCl as reference electrode. 10 mg of catalyst was suspended in 1 ml of 1 wt% Nafion solution and the mixtures were ultrasonically scattered for 1 min to form a homogeneous solution. Then, 0.2 ml solution was dropped on the fluorine doped tin oxide (FTO) glass (1.5×2 cm). After evaporation of the water in air, the catalysts were attached onto the surface of the FTO glass, which was used as the working electrode. Electrochemical impedance spectroscopy (EIS) was carried out at the open circuit potential. The amplitude of the sinusoidal wave was 1 mV, and frequency range was from 100 kHz to 1 Hz. The current–time (I–T) curves were collected at 0.5 V vs. SCE. During all measurements, the electrolyte was 0.1 M Na_2SO_4.

3. Results and discussion

3.1. Structural analysis

Fig. 1a shows the XRD patterns of the typical samples of WO_3 and H_xWO_3/WO_3. The XRD pattern of H_xWO_3/WO_3 is quite similar to that of pristine monoclinic WO_3. The hybrid material is composed of mainly monoclinic WO_3 (JCPDS: 43-1035) together with a small amount of H_xWO_3 (JCPDS: 20-0483) [12]. The six strong diffraction peaks from the hybrid sample shift slightly to higher diffraction angles compared to those of the pristine WO_3. Furthermore, as for the hybrid sample, two broad diffraction peaks are observed at 28.68° and 41.60°, while they did not exhibit in the WO_3 sample (detailed analysis see in Supplementary Table S1). It
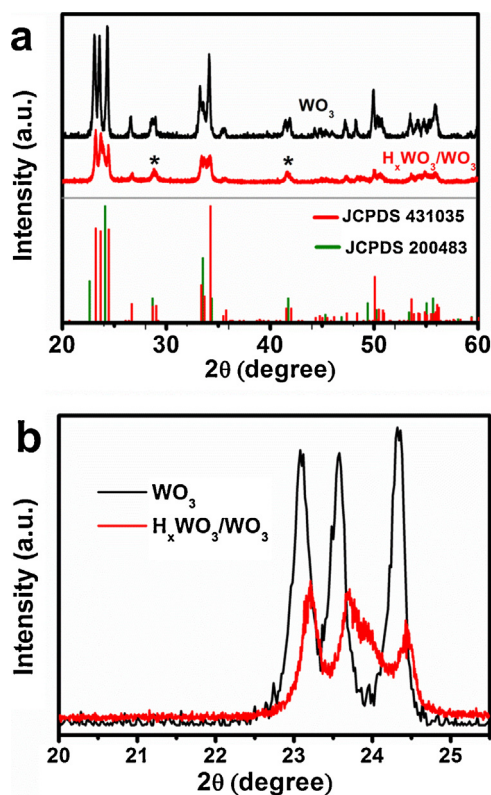

Fig. 1. (a) XRD patterns of WO_3 sample and H_xWO_3/WO_3 nanoheterostructure. (b) Magnified peaks in 2θ range from 20 to 26°.

indicates that a kind of phase formed in the hybrid sample. The XRD pattern of H_xWO_3/WO_3 sample can be indexed to the presence of both H_xWO_3 and WO_3. For the hybrid sample, a broad diffraction peak is observed at 28.68°, which indicates its smaller size.

As shown in TEM and HRTEM images (see in Supplementary Figs. S1 and S2.), the sizes of the H_xWO_3/WO_3 nanoheterostructure were in the range of 10–20 nm, which is accordance with the pore sizes of the as-prepared MCF template. On the other hand, the size of the H_xWO_3/WO_3 calculated by the Scherrer equation from the XRD data is ∼16.0 nm. The results of TEM and XRD implied the H_xWO_3/WO_3 were in situ formed in the pores of the MCF template. The narrow pores in the MCF template could supply advantageous environment to help alcohol to reduce the WO_3 [13].

Being a composition sample, the H_xWO_3/WO_3 appears green, which results from mixing of blue color of H_xWO_3 phase with yellow color of WO_3 body phase. Fig. 2a shows the UV–vis–NIR diffuse reflectance spectra (DRS) of the as-prepared H_xWO_3/WO_3 and sole

Fig. 2. (a) UV–vis diffuse reflectance spectra of WO_3 (I) and H_xWO_3/WO_3 (II). Inset: UV–vis–NIR diffuse reflectance spectra of H_xWO_3/WO_3 from 300 to 2500 nm. (b) FTIR spectra of WO_3 (black) and H_xWO_3/WO_3 (red). (c) Raman spectrum of pristine WO_3 and H_xWO_3/WO_3 samples. (For interpretation of the references to colour in this figure legend, the reader is referred to the web version of this article.)
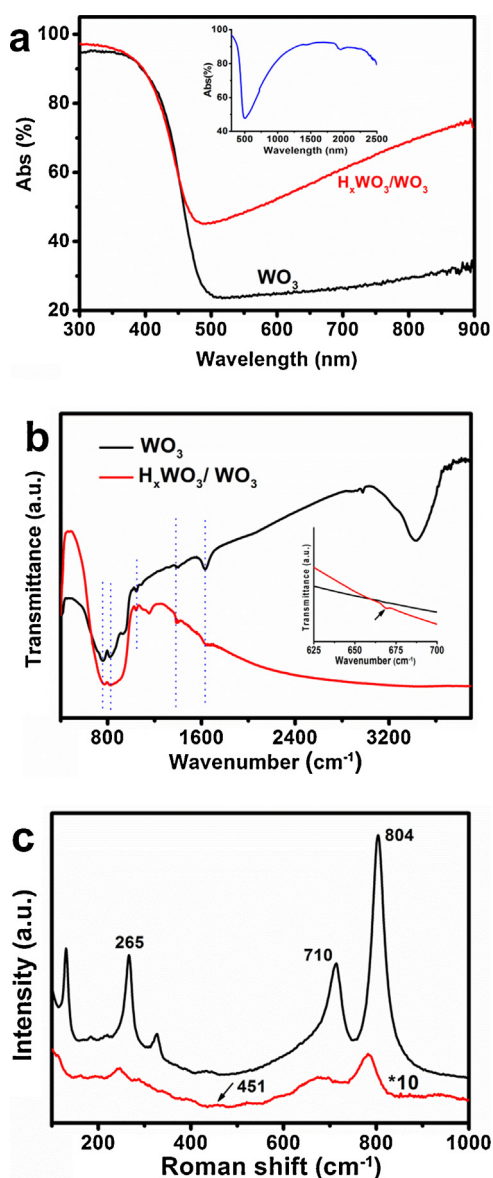
monoclinic WO_3 as a comparison. Both samples show fairly identical absorbance in the UV–vis region. The optical absorption of the H_xWO_3/WO_3 composite is consistent with indirect band gap absorption edge of the WO_3 (2.53 eV). Meanwhile, the absorbance of H_xWO_3/WO_3 increases significantly from wavelength of 480 nm up to 2000 nm. This is in agreement with the color changes from yellow of pure WO_3 to green of composite. It is generally accepted that the variable light absorption of tungsten oxide is caused by the change in its electronic structure, which is related to the change in the oxidation state of W atom, such as from W^{6+} to W^{5+} [7,14]. Hence, formation of low valence W species in H_xWO_3 is contributable to the light absorption in the near-infrared area.

Fig. 2b presents the FTIR spectrum of the as-prepared H_xWO_3/WO_3, together with that of monoclinic WO_3 for comparison. Since the vibrational spectroscopic methods are very sensitive to the local structural orders, the observed FTIR features in different materials can be considered as their distinctive structural features. For monoclinic WO_3, the most noteworthy band is a rather broad double dips at about 757 and 826 cm^{-1}, two much smaller but also broad dips at 1636 and 3432 cm^{-1}, and three small but sharp dips at 1049, 1393, and 1636 cm^{-1} [15]. All these features are retained for H_xWO_3/WO_3 except that the absence of any infrared absorption bands in the region 3000–3900 cm^{-1} and the appearance of a band at 670 cm^{-1}. The former was usually associated with constitutional hydroxyl group, and the latter located in a region usually associated with metal–hydrogen deformation motions [16]. More importantly, these characterizes were clearly observed as the characterized bands of H_xWO_3 by Sienko and Oesterreicher [17]. It confirms that a small amount of H_xWO_3 was formed in the as-prepared product.

Raman spectroscopy is a powerful tool for elucidation of structural and compositional features of semiconductor materials. Fig. 2c shows the characteristic Raman bands of monoclinic phase WO_3 and H_xWO_3. The Raman bands at 804 and 710 cm^{-1} are due to W—O—W stretching frequencies, and the band at 265 cm^{-1} is related to the W—O—W bending mode [18]. The sharp decrease in the Raman intensity for H_xWO_3/WO_3 can be associated with color center (tungsten ions in +5 valence state), which causes a strong decrease of the total Raman intensity due to optical absorption [14]. These results are agreed with the reported hydrogenated tungsten bronzes samples [19]. Considering the XRD patterns, FTIR spectrum, thermal behavior (see in Supplementary Fig. S3) and ESR (electron spin resonance) study (see in Supplementary Fig. S4), it can be inferred that the H_xWO_3/WO_3 composite has formed by our synthesis method.
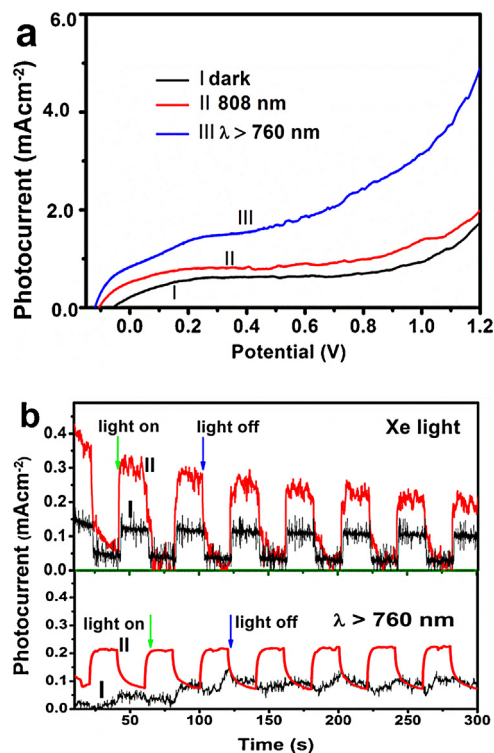
3.2. Photoactivity for methyl orange degradation

NIR photocatalytic activity of the hybrid H_xWO_3/WO_3 composite was measured under different light irradiation. Experiments on degradation ability of light irradiation without the photocatalyst confirm that the light irradiation could not induce methyl orange (MO) degradation. In Fig. 3a, except for the good visible photocatalytic activity, we found that MO could be degraded in the H_xWO_3/WO_3 aqueous solution under NIR light irradiation. Degradation rates of MO over the H_xWO_3/WO_3 under full spectra of Xe lamp, visible (≤760 nm), and near-infrared light (≥760 nm) irradiation for 120 min are 88%, 66% and 24%, respectively. Time courses of MO degradation over the H_xWO_3/WO_3 composite irradiated by LED (3 W, 630 nm) are shown in Fig. 3b. In comparison to the dark reaction, MO molecules indeed were degraded after 24 h irradiation, which confirmed the photocatalytic activity induced by the H_xWO_3 component in the nanoheterostructure. Cyclic experiments on photocatalytic performance of H_xWO_3/WO_3 composite demonstrate that the samples exhibited stable performance, i.e. there was
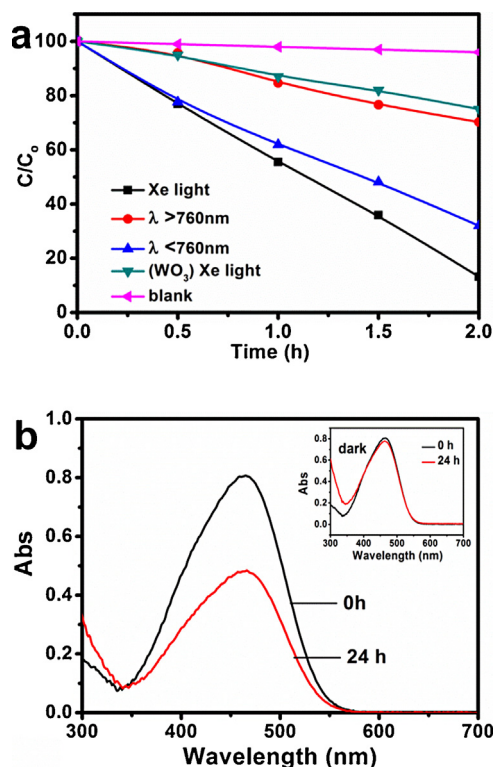
Fig. 3. (a) Photodegradation curves of MO at different conditions. (b) Temporal UV–vis absorption spectra changes of MO under the irradiation of LED (630 nm, 3 W).

Fig. 4. (a) Typical I–V curves of the H_xWO_3/WO_3 in dark (curve I) and under illumination with the different light (red (II): 3 mW 808 nm laser; blue (III): 500w Xe lamp cut off by filter of 760 nm) in 0.5 M Na_2SO_4. (b) I–T curves under chopped light illumination of WO_3 (black curve(I)) and H_xWO_3/WO_3 (red curve(II)) in 0.5 M Na_2SO_4. The scan rate was 10 mV/s. (For interpretation of the references to colour in this figure legend, the reader is referred to the web version of this article.)

no obvious decrease in photocatalytic degradation activity even after five cycles (see in Supplementary Fig. S5).

3.3. Photoelectrochemical properties for H_xWO_3/WO_3 nanoheterostructure

Linear scan voltammetry was performed in the dark and under different light irradiation to examine the light response of the H_xWO_3/WO_3. As shown in Fig. 4a, photocurrent increases with increasing of irradiation power, which is attributed to increasing density of photogenerated electrons induced by the light irradiation. To clearly observe variation trend of the photocurrent for the H_xWO_3/WO_3 composite and the pure WO_3 with and without the light irradiation, the photocurrent with chopped light is shown in Fig. 4b. The change of the photocurrent of the H_xWO_3/WO_3 composite sample is significant under full spectra as well as NIR irradiation. However, the pure WO_3 did not show obvious response or a change with the NIR light irradiation. It suggests that the H_xWO_3 could be irradiated by the NIR and then to increase the photocurrent. In addition, the difference of the photocurrent between the two samples may come from high electrical conductivity of the H_xWO_3. Fig. S6 shows electrochemical impedance spectra (EIS) Nyquist plots of WO_3 and H_xWO_3/WO_3 electrodes with or without light irradiation. Diameter of arc radius on the EIS Nyquist plot of the H_xWO_3/WO_3 is smaller than that of the WO_3 regardless of whether it is with or without light irradiation, which implies the higher efficiency of charge transfer in H_xWO_3/WO_3.

3.4. Mechanism of the enhanced photocatalytic activity

The above results may be closely related to the metallic character of the H_xWO_3 component. Hydrogen atom insertion in the bulk of WO_3 causes a change in electronic structure of the material, introducing occupied defects states near bottom of the conduction band (CB) [20]. The hydrogen forms a hydroxide unit with one oxygen atom, and induces an oxygen vacancies defect band, which caused an upshift of the Fermi level and increased the intensive full-spectrum absorption [3,7,19,21]. The oxygen vacancies provided trapping sites to trap electrons. As a result, lifetime of the photoexcited electrons was prolonged (proved by the Fluorescence emission decay spectra, Fig. S7), thus promoting the separation of the photo-generated carriers. On the other hand, the dispersed defect state merges with the conduction band, leading to a metallic or very high semiconductivity character of the system which is advantageous for the transfer of the carriers. Thus, the H_xWO_3 on the WO_3 phase is helpful for enhancing the light absorption and transfer of the carriers, though it was reported that H_xWO_3 itself was incapable of photocatalytic O_2 evolution [19].

To approach mechanism of enhancing photocatalytic activity of the H_xWO_3/WO_3 composite, the relative band positions of the two semiconductors were investigated, since the band-edge potential levels play a crucial role in determining flowchart of photoexcited charge carriers in a heterojunction. The minimum CB of H_xWO_3 is obviously lower than that of the WO_3 according to the theory calculation [7,18]. It indicated the composite of H_xWO_3/WO_3 was advantageous for the separation and transportation of charge carriers. As illustrated in Fig. 5, under visible light irradiation, both the WO_3 and H_xWO_3 are easily excited and generate photo-induced electrons and holes correspondingly. In addition, the photo-induced electrons and holes are also generated in the H_xWO_3 under NIR light irradiation (process 1, 2 in Fig. 5, respectively). Photogenerated electrons are injected with high efficiency from the conduction band of WO_3 to the conduction band of H_xWO_3 because of the intimate contact between the two semiconductors (process 3 in Fig. 5). Meanwhile, the photoexcited electrons and holes with high energy may cool down to
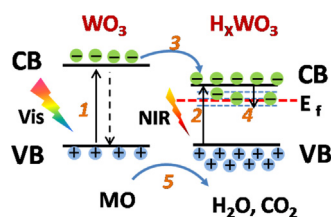
Fig. 5. A schematic representation of the photocatalysis mechanism of H_xWO_3/WO_3 under the light irradiation.

the conductive band edges of the H_xWO_3 or relax to the defect sites (process 4 in Fig. 5). The transfer of charge carrier to H_xWO_3 may lead to charge separation, which would suppress radiative recombination of the electrons and holes. In such a way, the photo-induced electrons and holes can be efficiently separated, and the recombination of electron–hole pairs can be reduced in accordance with result of the PL spectra (inset of Fig. S7). Therefore, the efficient transfer of electrons could greatly decrease the probability of photo-excited electron–hole recombination. Increasing the lifetime of photo-excited holes on the valence band of WO_3 and H_xWO_3 would result in the high photocatalytic activity to degradation the organic dye (MO) (process 5 in Fig. 5).

4. Conclusion

In summary, the metallic/semiconducting H_xWO_3/WO_3 nanoheterostructure exhibits high photocatalytic activity to degrade MO in aqueous solution under broad spectrum irradiation. The hybrid H_xWO_3/WO_3 nanoheterostructure displays the photocurrent under NIR irradiation. The high NIR absorption of the composite was attributed to the introduced defection level at the bottom of the conduction band in the non-stoichiometric H_xWO_3. It is proposed that the fast electron transfer from WO_3 to H_xWO_3 nanoparticle is responsible for the improvement in photocatalytic activity. This result is of significance in utilization of all solar band energy, especially for NIR light, which constitutes a considerable part of sunlight.

Appendix A. Supplementary data

Supplementary data associated with this article can be found, in the online version, at http://dx.doi.org/10.1016/j.apcatb.2014.12.018.

References

[1] A.V. Akimov, A.J. Neukirch, O.V. Prezhdo, Chem. Rev. 113 (2013) 4496–4565.
[2] T.L. Thompson, J.T. Yates Jr., Chem. Rev. 106 (2006) 4428–4453.
[3] G. Liu, L.Z. Wang, H.G. Yang, H.M. Cheng, G.Q. Lu, J. Mater. Chem. 20 (2010) 831–843.
[4] C. Guo, S. Yin, P. Zhang, M. Yan, K. Adachi, T. Chonan, T. Sato, J. Mater. Chem. 20 (2010) 8227–8229.
[5] L. Wang, J. Zhan, W. Fan, G. Cui, H. Sun, L. Zhuo, X. Zhao, B. Tang, Chem. Commun. 46 (2010) 8833.
[6] C. Guo, S. Yin, L. Huang, T. Sato, ACS Appl. Mater. Interfaces 3 (2011) 2794–2799.
[7] A. Hjelm, C.G. Granqvist, J.M. Wills, Phys. Rev. B 54 (1996) 2436–2445.
[8] M. Whittingham, Solid State Ionics 168 (2004) 255–263.
[9] Y. Xi, Q. Zhang, H. Cheng, J. Phys. Chem. C 118 (2014) 494–501.
[10] Y. Han, J.Y. Ying, Angew. Chem. Int. Ed. 44 (2005) 288–292.
[11] D.J. Ham, A. Phuruangrat, S. Thongtem, J.S. Lee, Chem. Eng. J. 165 (2010) 365–369.
[12] P.G. Dickens, R.J. Hurditch, Nature 215 (1967) 1266–1267.
[13] S. Ayyappan, C.N.R. Rao, Mater. Res. Bull. 30 (1995) 947–951.
[14] O.F. Schirmer, V. Wittwer, G. Baur, G. Brandt, J. Electrochem. Soc. 124 (1977) 749–753.
[15] M.F. Daniel, B. Desbat, J.C. Lassegues, B. Gerand, M. Figlarz, J. Solid State Chem. 67 (1987) 235–247.
[16] M.L.H. Green, D.J. Jones, Adv. Inorg. Radio Chem. 7 (1965) 133.
[17] M.J. Sienko, H. Oesterreicher, J. Am. Chem. Soc. 90 (1968) 6568–6570.
[18] E. Cazzanelli, C. Vinegoni, G. Mariotto, A. Kuzmin, J. Purans, Solid State Ionics 123 (1999) 67–74.
[19] G. Liu, J. Han, X. Zhou, L. Huang, F. Zhang, X. Wang, C. Ding, X. Zheng, H. Han, C. Li, J. Catal. 307 (2013) 148–152.
[20] C. Di Valentin, F. Wang, G. Pacchioni, Top. Catal. 56 (2013) 1404–1419.
[21] P.G. Dickens, J.H. Moore, D.J. Neild, J. Solid State Chem. 7 (1973) 241–244.